Supplemental Material for "Measurement of the Cross Section for $e^+e^- \to \Lambda\bar{\Lambda}$ and Evidence of the Decay $\psi(3770) \to \Lambda\bar{\Lambda}$"

TABLE I. The $e^+e^- \to \Lambda\bar{\Lambda}$ cross section and effective form factor for 33 energy points between 3.51 and 4.6 GeV. The first uncertainties are statistical, and the second ones are systematic uncertainties. The $\sqrt{s}$ is the e^+e^- center-of-mass energy [1]. The $\mathcal{L}$ is the integrated luminosity of each data set (note that the luminosities for some of energy points are preliminarily measured with the same method as Ref. [2]), the vacuum polarization correction factor $\frac{1}{|1-\Pi|^2}$, the ISR correction factor $1+\delta$, the detection efficiency ϵ. The N_S is from the signal region, N_{bkg} is the number of background events scaled by sideband region, N_{obs} is the number of observed events by subtracting the backgrounds with the uncertainty calculated by Feldman Cousins in Ref. [3], (the number of signal events for the upper limit with the consideration of systematic uncertainty estimated based on TRolke method [4]) $N_{\rm obs}$. The Born cross section σ^B, the effective form factor $|G_{\rm eff}(s)|$ and statistical significances $S(\sigma)$ for 33 energy points are summarized in Table I. The values in the brackets are the corresponding upper limits at 90% C.L..

$\sqrt{s}$ (GeV)	$\mathcal{L}$ (pb^{-1})	$\frac{1}{\lvert 1-\Pi\rvert^2}$	$1+\delta$	$\epsilon(\%)$	N_S	N_{bkg}	N_{obs}	σ^B (fb)	$\lvert G_{\rm eff}(s)\rvert \times 10^{-3}$	S(σ)
3.5100	405.4	1.04	0.96	36.21 ± 0.19	61.0	0.0	$61.0^{+7.8}_{-7.8}$	$1020^{+130}_{-130} \pm 44$	$12.5^{+0.8}_{-0.8} \pm 0.4$	7.8
3.5146	41.1	1.04	0.96	36.38 ± 0.19	5.0	0.0	$5.0^{+2.8}_{-2.2}$ (< 9.7)	$820^{+460}_{-360} \pm 35$ (< 1600)	$11.2^{+3.1}_{-2.5} \pm 0.3$ (< 15.6)	2.2
3.5815	85.7	1.04	1.01	34.41 ± 0.18	13.0	0.0	$13.0^{+4.3}_{-3.7}$	$1030^{+340}_{-290} \pm 44$	$12.7^{+2.1}_{-1.8} \pm 0.4$	3.6
3.6500	44.0	1.04	1.07	31.98 ± 0.18	3.0	0.0	$3.0^{+2.3}_{-1.9}$ (< 6.8)	$470^{+360}_{-230} \pm 20$ (< 1000)	$8.7^{+3.4}_{-2.8} \pm 0.3$ (< 13.2)	1.7
3.6702	84.7	1.04	1.09	31.23 ± 0.18	10.0	0.0	$10.0^{+3.8}_{-3.2}$	$790^{+370}_{-250} \pm 34$	$11.4^{+2.8}_{-1.8} \pm 0.4$	3.2
3.7730	2916.9	1.06	1.16	33.70 ± 0.18	262.0	1.3	$261.0^{+16.2}_{-16.2}$	$530^{+33}_{-33} \pm 22$	$9.6^{+0.3}_{-0.3} \pm 0.3$	16.0
3.8077	50.54	1.06	1.20	33.29 ± 0.18	2.0	0.0	$2.0^{+2.3}_{-1.3}$ (< 5.3)	$230^{+260}_{-150} \pm 10$ (< 610)	$6.3^{+3.6}_{-2.1} \pm 0.2$ (< 10.3)	1.4
3.8675	108.9	1.05	1.25	32.91 ± 0.18	1.0	0.0	$1.0^{+1.8}_{-0.6}$ (< 3.7)	$52^{+94}_{-31} \pm 2$ (< 190)	$3.1^{+2.8}_{-0.9} \pm 0.1$ (< 5.9)	1.0
3.8715	110.0	1.05	1.25	32.78 ± 0.18	2.0	0.3	$1.7^{+2.3}_{-0.9}$ (< 5.3)	$88^{+120}_{-47} \pm 4$ (< 270)	$4.0^{+2.7}_{-1.1} \pm 0.1$ (< 7.0)	1.0
3.8962	52.61	1.05	1.27	31.04 ± 0.18	1.0	0.0	$1.0^{+1.8}_{-0.6}$ (< 3.7)	$110^{+200}_{-68} \pm 5$ (< 420)	$4.5^{+4.1}_{-1.4} \pm 0.1$ (< 8.7)	1.0
4.0076	482.0	1.05	1.47	26.38 ± 0.17	13.0	0.0	$13.0^{+4.3}_{-3.7}$	$160^{+54}_{-46} \pm 7$	$5.6^{+0.9}_{-0.8} \pm 0.2$	3.6
4.1301	390.0	1.05	1.46	20.80 ± 0.16	7.0	1.0	$6.0^{+3.3}_{-2.7}$ (< 10.0)	$120^{+65}_{-53} \pm 5$ (< 200)	$4.9^{+1.3}_{-1.1} \pm 0.2$ (< 6.3))	2.3
4.1585	410.4	1.05	1.50	24.10 ± 0.15	8.0	0.3	$7.7^{+3.3}_{-2.7}$ (< 13.7)	$120^{+52}_{-43} \pm 5$ (< 220)	$5.0^{+1.1}_{-0.9} \pm 0.2$ (< 6.7)	2.7
4.1783	3189.0	1.05	1.54	21.53 ± 0.15	20.0	2.0	$18.0^{+5.3}_{-4.2}$	$40^{+12}_{-9} \pm 2$	$2.9^{+0.4}_{-0.3} \pm 0.1$	4.0
4.1893	526.7	1.06	1.56	21.00 ± 0.14	1.0	0.5	$0.5^{+1.8}_{-0.5}$ (< 3.7)	$7^{+24}_{-7} \pm 1$ (< 50)	$1.2^{+2.1}_{-0.6} \pm 0.1$ (< 3.2)	1.0
4.1996	526.0	1.06	1.38	21.14 ± 0.14	4.0	0.3	$3.7^{+2.8}_{-1.7}$ (< 8.3)	$56^{+42}_{-26} \pm 2$ (< 130)	$3.4^{+1.3}_{-0.8} \pm 0.1$ (< 5.1)	1.9
4.2097	517.1	1.06	1.39	20.26 ± 0.14	1.0	0.0	$1.0^{+1.8}_{-0.6}$ (< 3.7)	$16^{+29}_{-10} \pm 1$ (< 59)	$1.8^{+1.6}_{-0.6} \pm 0.1$ (< 3.5)	1.0
4.2188	514.6	1.06	1.40	20.17 ± 0.13	1.0	0.3	$0.7^{+1.8}_{-0.6}$ (< 3.7)	$11^{+29}_{-10} \pm 1$ (< 59)	$1.5^{+2.0}_{-0.7} \pm 0.1$ (< 3.5)	1.2
4.2263	1056.4	1.06	1.41	21.31 ± 0.14	17.0	0.3	$16.7^{+4.4}_{-3.8}$	$120^{+32}_{-30} \pm 5$	$5.1^{+0.7}_{-0.6} \pm 0.2$	4.0
4.2358	530.3	1.06	1.43	20.66 ± 0.14	5.0	0.5	$4.5^{+2.8}_{-2.3}$ (< 9.7)	$66^{+41}_{-34} \pm 3$ (< 140)	$3.8^{+1.2}_{-1.0} \pm 0.1$ (< 5.5)	2.0
4.2439	538.1	1.06	1.69	20.35 ± 0.14	3.0	0.3	$2.7^{+2.3}_{-1.8}$ (< 6.8)	$34^{+29}_{-23} \pm 2$ (< 85)	$2.7^{+1.1}_{-0.9} \pm 0.1$ (< 4.3)	1.6
4.2580	828.4	1.05	1.72	20.54 ± 0.14	6.0	0.0	$6.0^{+3.3}_{-2.2}$ (< 11.0)	$48^{+26}_{-18} \pm 2$ (< 88)	$3.2^{+0.9}_{-0.6} \pm 0.1$ (< 4.3)	2.4
4.2669	531.1	1.05	1.74	20.15 ± 0.15	2.0	0.0	$2.0^{+2.3}_{-1.3}$ (< 5.3)	$25^{+29}_{-16} \pm 1$ (< 66)	$2.3^{+1.3}_{-0.8} \pm 0.1$ (< 3.8)	1.4
4.2778	157.7	1.05	1.75	18.88 ± 0.13	1.0	0.0	$1.0^{+1.8}_{-0.6}$ (< 3.7)	$40^{+72}_{-24} \pm 2$ (< 150)	$3.0^{+2.7}_{-0.9} \pm 0.1$ (< 5.7)	1.0
4.2889	500.0	1.05	1.71	19.46 ± 0.14	7.0	0.0	$7.0^{+3.3}_{-2.7}$ (< 12.4)	$98^{+46}_{-38} \pm 4$ (< 170)	$4.6^{+1.1}_{-0.9} \pm 0.1$ (< 6.2)	2.6
4.3128	497.4	1.05	1.75	19.29 ± 0.14	5.0	0.3	$4.7^{+2.8}_{-2.2}$ (< 9.7)	$65^{+39}_{-31} \pm 3$ (< 130)	$3.8^{+1.1}_{-0.9} \pm 0.1$ (< 5.5)	2.1
4.3379	512.1	1.05	1.80	19.36 ± 0.13	3.0	0.3	$2.7^{+2.3}_{-1.8}$ (< 6.8)	$35^{+43}_{-24} \pm 2$ (< 89)	$2.8^{+1.7}_{-0.8} \pm 0.1$ (< 4.5)	1.6
4.3583	543.9	1.05	1.67	18.58 ± 0.13	4.0	0.3	$3.7^{+2.8}_{-1.7}$ (< 8.3)	$51^{+39}_{-24} \pm 2$ (< 110)	$3.4^{+1.3}_{-0.8} \pm 0.1$ (< 5.1)	1.9
4.3776	532.9	1.05	1.88	18.44 ± 0.13	2.0	0.8	$1.2^{+2.3}_{-1.0}$ (< 5.3)	$15^{+29}_{-13} \pm 1$ (< 67)	$1.9^{+1.8}_{-0.8} \pm 0.1$ (< 3.9)	1.1
4.3980	516.0	1.05	1.93	17.68 ± 0.13	0.0	0.5	$0.0^{+0.8}_{-0.0}$(< 2.0)	$0^{+11}_{-0} \pm 1$ (< 27)	< 2.5	...
4.4156	1043.9	1.05	1.98	17.20 ± 0.12	3.0	0.5	$2.5^{+2.3}_{-1.7}$ (< 6.8)	$16^{+15}_{-11} \pm 1$ (< 45)	$1.9^{+0.9}_{-0.6} \pm 0.1$ (< 3.2)	1.4
4.4370	582.7	1.05	2.02	16.70 ± 0.12	5.0	0.0	$5.0^{+2.8}_{-2.2}$ (< 9.7)	$59^{+33}_{-26} \pm 3$ (< 120)	$3.7^{+1.0}_{-0.8} \pm 0.1$ (< 5.2)	2.2
4.5995	586.9	1.05	2.25	13.96 ± 0.11	1.0	0.3	$0.7^{+1.8}_{-0.6}$ (< 3.7)	$9^{+23}_{-8} \pm 1$ (< 47)	$1.5^{+1.9}_{-0.6} \pm 0.1$ (< 3.4)	1.2

[1] M. Ablikim *et al.* (BESIII Collaboration), Chin. Phys. C **40**, 063001 (2016).
[2] M. Ablikim *et al.* (BESIII Collaboration), Chin. Phys. C **39**, 093001 (2015).
[3] G. J. Feldman and R. D. Cousins, Phys. Rev. D **57**, 3873 (1998).
[4] J. Lundberg, J. Conrad, W. Rolke and A. Lopez, Comput. Phys. Commun. **181**, 683 (2010).

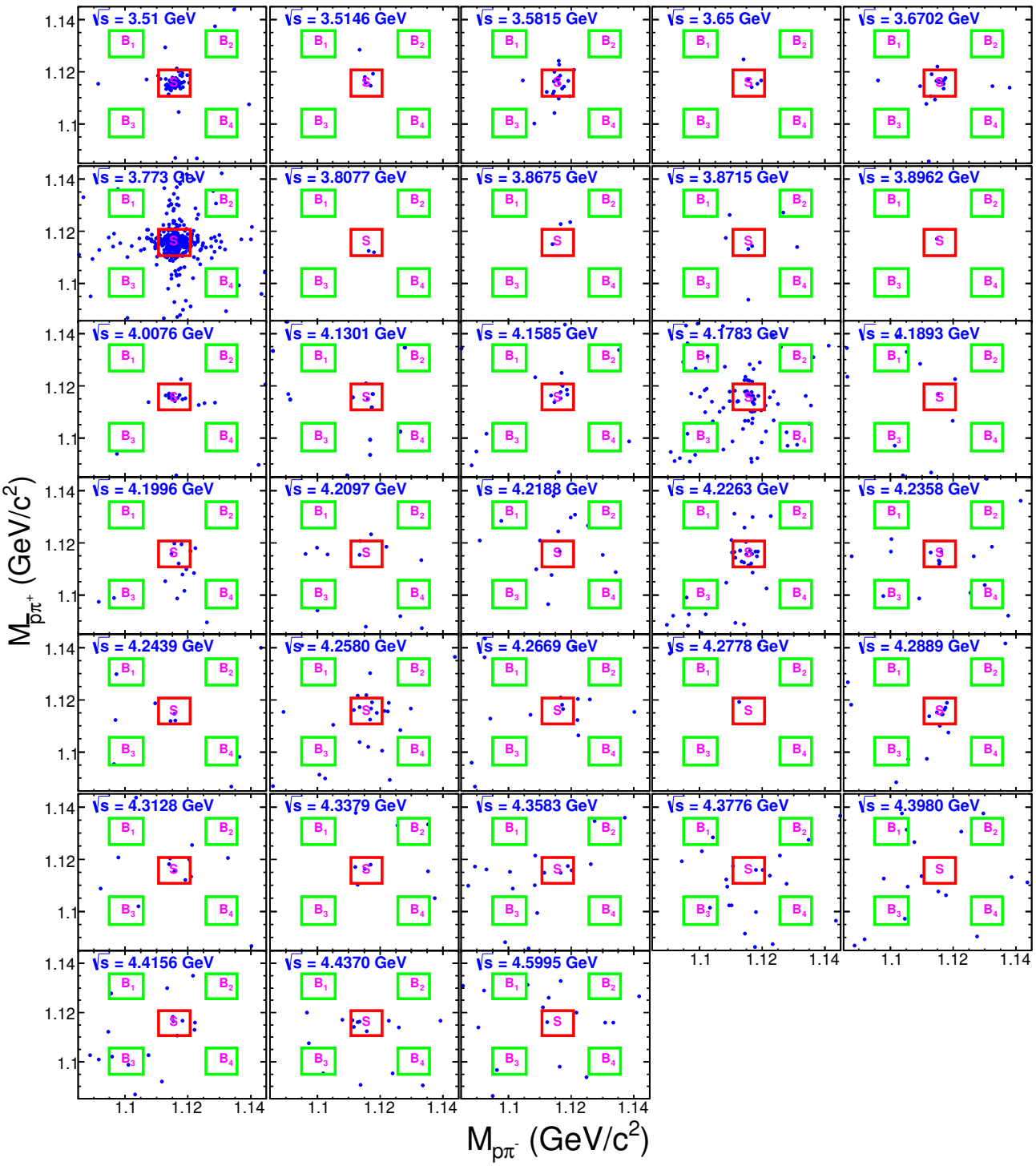

FIG. 1. Distribution of $M_{p\pi^-}$ versus $M_{\bar{p}\pi^+}$ for all 33 energy points between 3.51 and 4.60 GeV for all 33 energy points in data, where the red box stands for the signal region, the green boxes denote the selected sideband regions. The sideband regions are denoted by B_i, where i runs over the four regions: $B_1 \in [1.0957, 1.1057]$ GeV/c^2 & $[1.1257, 1.1357]$ GeV/c^2, $B_2 \in [1.1257, 1.1357]$ GeV/c^2 & $[1.1257, 1.1357]$ GeV/c^2, $B_3 \in [1.0957, 1.1057]$ GeV/c^2 & $[1.0957, 1.1057]$ GeV/c^2, $B_4 \in [1.1257, 1.1357]$ GeV/c^2 & $[1.0957, 1.1057]$ GeV/c^2.